ACCELERATED WEATHERING OF THE MATRIX

This fifth chapter is devoted to the cementitious matrix. The first part deals with the characterization of hydrated cement paste before the weathering. The second part presents the development of a method to accelerate matrix weathering: accelerated carbonation operation and leaching operation. Finally, the influence of accelerated weathering of the matrix on its microstructure is discussed in the third part.

1. Characterization of hydrated cement paste

1.1. X-ray diffraction (XRD) analysis

The XRD analysis of hydrated cement paste is presented in Figure 19. The assignments of the XRD peaks to phases were based on 2θ values and the corresponding d-spacing (Table 1).

Table 1: XRD Data for hydrated cement paste at 28 days of curing at 100% HR

2 θ	d (Å)	Phase	2 θ	d (Å)	Phase
9.3	9.671	Ettringite	34.0	2.628	Portlandite
16.1	5.583	Ettringite	47.1	1.927	Portlandite
18.1	4.900	Portlandite	51.5	1.796	Portlandite
23.3	3.859	Ettringite	55.1	1.687	Portlandite
28.7	3.112	Portlandite			

Diffractogram investigation indicates that the hydrated cement paste studied is mainly composed of portlandite, and ettringite. The peaks corresponding to portlandite appear at 4.900, 3.112, 2.628, 1.927, 1.796, and 1.687 Å. The main peaks corresponding to ettringite are present at 9.671, 5.583, and 3.859 Å. Presence of calcite ($CaCO_3$) and gypsum can be observed but at a lower extent.

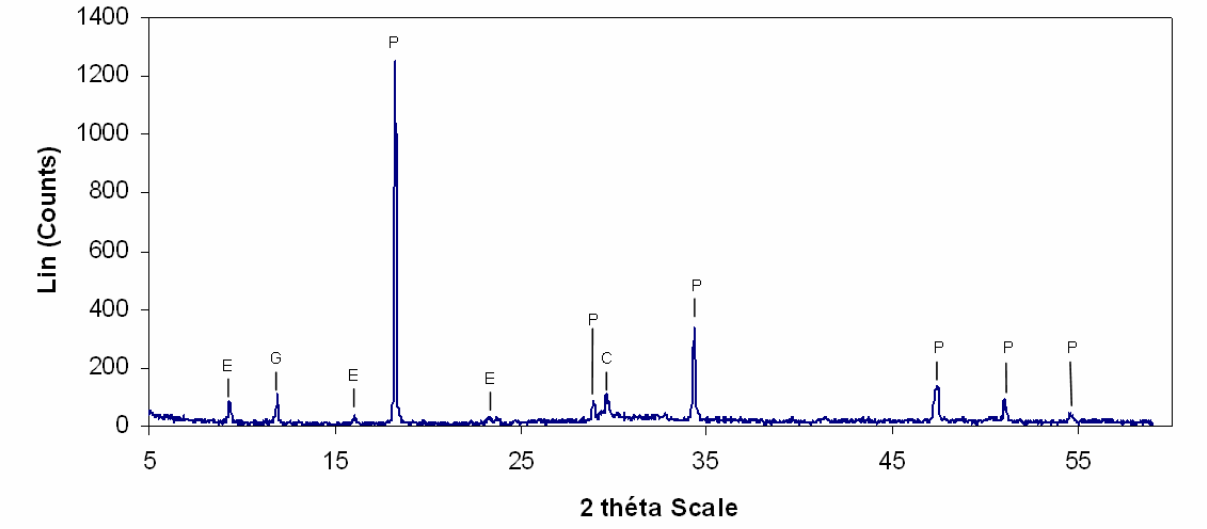

Figure 19: X-ray diffractogram of hydrated cement paste at 28 days of curing at 100% RH
E=ettringite, G=gypsum, P=portlandite, C=calcite

1.2. Fourier Transformed infrared (FT-IR) analysis

FT-IR spectra of hydrated cement paste are shown in Figure 20 and Figure 21. Usually band assignments reported in literature are deducted from spectra performed in diffuse reflectance.

Table 2: FT-IR characterization of hydrated cement paste

Band assignements	Hydrated cement[a] 1 month (cm^{-1})	Hydrated cement[b] after mixing (cm^{-1})	Hydrated cement [c] paste (cm^{-1})	Hydrated cement [d] paste (cm^{-1})
ν_3 SiO_4^{4-}	980 s, b	970 s, b	977 s, b	959 s
ν_4 SiO_4^{4-}	536 w, sh	------	------	------
ν_2 SiO_4^{4-}	467 s	------	453 w	446 w
ν_3 SiO_4^{2-}	1105 w, sh	1100	1134 vw, sh	1113 vw, sh
	1155 w, sh	------	------	------
ν_4 SiO_4^{2-}	667 w	610	------	------
$\nu_1 + \nu_3$ H_2O	3325	------	------	------
	3450 s, b	3415 s, b	3436 s, b	3414 m, b
ν_2 H_2O	1630 w	1638 m	1656 m	1640 w
ν OH^-	3645 sr, sh	3640 sr	3644 sr, sh	3636 sr, sh
ν_3 CO_3^{2-}	1425 1497 s, b	1421 s, b	1462 s, b	1414 s
ν_2 CO_3^{2-}	876 m, sr	874 m, sr	875 m, sr	872 s, sr
ν_4 CO_3^{2-}	732 w	713 w	718 w	710 w

[a] Reference Mollah et al., 1995; 2004
[b] Reference Farcas and Touzé, 2001
[c] Present study diffuse reflectance
[d] Present study ATR
b: broad, s: strong, sh: shoulder, sr: sharp, m: medium, vw: very weak, w: weak
$\nu 1$ = symmetric stretching
ν_2 = symmetric bending
ν_3 = asymmetric stretching
ν_4 = asymmetric bending

In the present work, spectra acquisition is mainly performed in ATR. Band assignments on ATR spectrum (Figure 21) are deducted from spectrum performed first in diffuse reflectance (Figure 20).

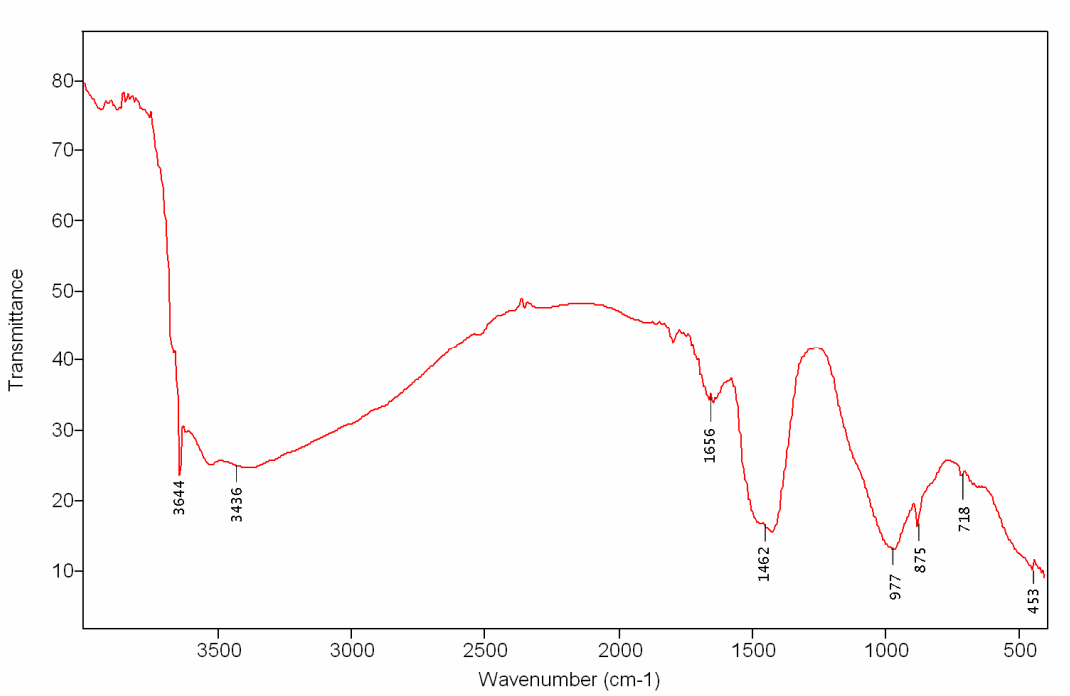

Figure 20: Diffuse reflectance FT-IR spectrum of hydrated cement paste at 28 days of curing at 100% RH

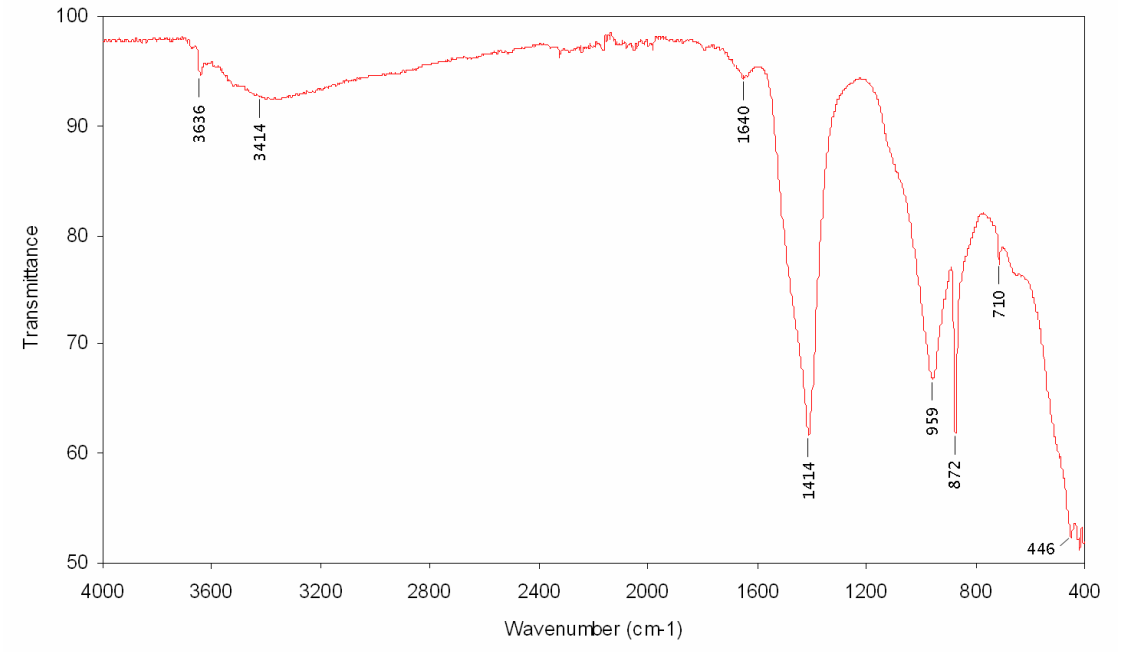

Figure 21: ATR FT-IR spectrum of hydrated cement paste at 28 days of curing at 100% RH

A shift of about 10-20 wave number units is noted between both spectra. Nevertheless the band assignments for hydrated cement paste are in close agreement with those previously reported by Mollah et al., 1995; 2004; and Farcas and Touzé, 2001 (Table 2). The band at 3645 cm^{-1} is due to the OH band from $Ca(OH)_2$ (Mollah et al., 2000). The water bands appear at approximately 3440 (stretching) and 1660 (bending) cm^{-1} (Mollahet al., 1998). The bands at 1480-1430 cm^{-1}, 875 cm^{-1} and 720 cm^{-1} are due to carbonates. The wide and deep band between 1480 and 1430 cm^{-1} is attributed to ν_3 of CO_3^{2-} and the sharp bands at 875 and 720 cm^{-1} are due to ν_2 and ν_4 vibrations, respectively (Mollah, 1998). The band at 975 cm^{-1} is due to the Si-O asymmetric stretching band (ν_3) from C-S-H (Mollah et al., 1995).

1.3. Mercury Intrusion Porosimetry (MIP)

In the usual procedure, a small specimen is first dried emptying the pores of any existing fluid. It is then weighed, transferred to a chamber, where the air is evacuated. Then mercury fills this chamber surrounding the specimen. Since mercury does not wet cementitious solids spontaneously, it does not intrude into empty pores unless pressure is applied. Therefore pressure in progressive increments is then applied. The intrusion of mercury at each step is monitored. The set of pressure steps and corresponding volumes intruded provides the basic data for pore size distribution calculation. The Washburn model used to convert mercury intrusion data into pore size distribution curves invokes two distinct assumptions: (i) that pores are cylindrical, and (ii) that they are entirely and equally accessible to the outer surface of the specimen. There is no distinction in the model between intrusion into a single long, continuous cylinder or intrusion into a multitude of shorter cylinders of the same diameter, as long as they are all open to the outer surface (Diamond, 2000). The access to large regions of porosity may be controlled by very small size entries and all the pores in this region (whatever their actual size) will be assigned to the size of the smallest entry (Scrivener, 2004). So, MIP data should be investigated and interpreted with care.

According to Diamond (2000), MIP measurements are useful only to provide threshold diameters and intrudable pore space measurements, which can serve as comparative indices for the connectivity and capacity of the pore systems in hydrated cements. MIP measurements should be abandoned as measures of the actual pore size present.

The apparent threshold diameter corresponds to a pressure above which very little intrusion into specimen is recorded, and immediately below which the greatest portion of intrusion

takes place. This apparent threshold diameter is greater for higher water: cement (w/c) ratios and for younger cement pastes; reducing with age (Diamond, 2000).

Pore size distribution of the hydrated cement paste studied is presented in Figure 22. The threshold diameter obtained is about 2 µm, that is to say that essentially all of the space can be allocated to pores less than 2 µm in size. The total porosity corresponding to the MIP measurements is of 21.6%.

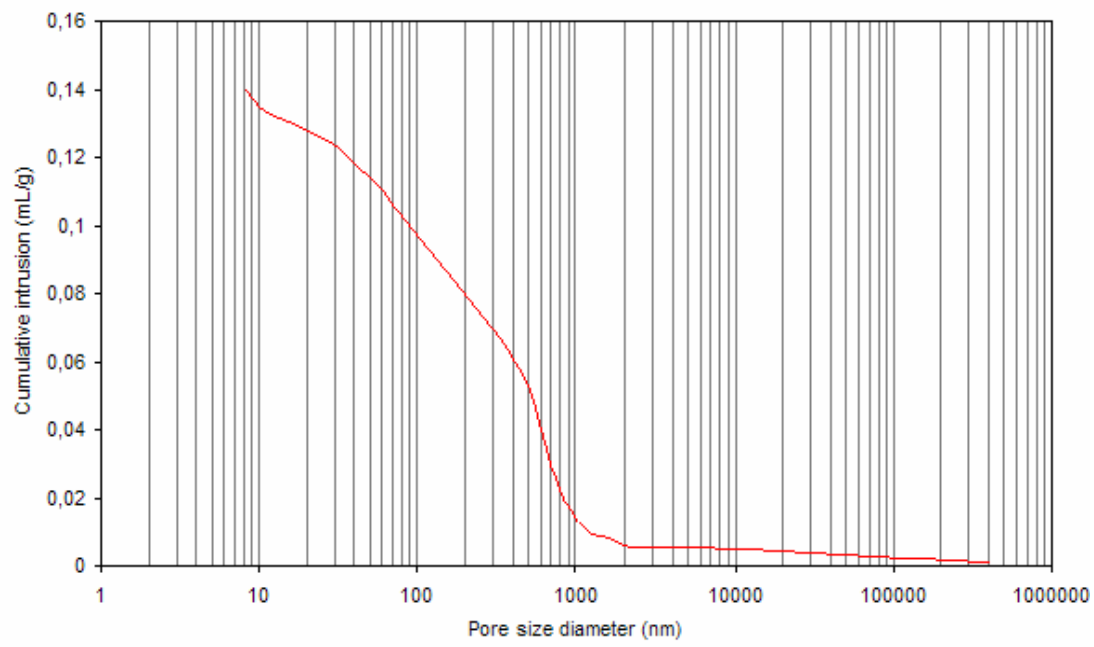

Figure 22: Pore size distribution of hydrated cement paste at 28 days of curing at 100% RH

1.4. Helium pycnometry

Usually, helium pycnometry is used to determine skeletal density of a solid, and could give indirect information about pore volume and closed porosity when the sample's apparent volume and density are known. In our case the specimens are shaped irregularly, so it is not quite as easy to determine their apparent volume. Hence, only skeletal bulk density is obtained from pycnometry measurements performed. The skeletal density of hydrated cement paste measured is to 2.197 ± 0.002 g/cm^3 after 28 days of curing at 100% RH.

A synthesis of XRD and FT-IR analyses indicates that the major components in hydrated cement are portlandite $Ca(OH)_2$, calcium-silica-hydrate C-S-H. The formation of ettringite - C_3A, 3 $CaSO_4$, H_{32} -, and calcite $CaCO_3$ is also observed. These observations are in close agreement with previous publication. Upon hydration the alite (C_3S) and belite (C_2S) phases

produce mainly portlandite $Ca(OH)_2$ (20-25%) and amorphous calcium-silica-hydrate (C-S-H) (60-70%) (Mollah, 1998). Calcium carbonate $CaCO_3$ is also produced as a result of secondary reactions between $CaOH_2$ and C-S-H with atmospheric CO_2 (Reardon et al., 1989). The hydrated cement paste studied is also characterized by: (i) a threshold diameter of 2 µm, (ii) a total porosity of 21.6%, and (iii) a skeletal density of 2.197 g/cm^3.

2. Accelerated weathering of the matrix

2.1. Accelerated carbonation

The accelerated carbonation is performed on hydrated cement pastes after 28 days of curing at 100% RH. Prior to exposure to carbonation, the majority of specimens (four exceptions) were oven dried at 40°C for 24h. The saturated solution of potassium carbonate is renewed after 30h. Hence, RH is maintained between 52% and 65% in the chamber. This saturated salt solution is known to provide 43% RH at 20°C when in an enclosed space (OIML R 121, 1996). In the experimental set-up, CO_2 bubbled through a column of deionised water before entering the inlet chamber, providing continuously humidity. Thus, RH is maintained in the chamber at a higher value than the one expected. According to Chaussadent (1997) and Gervais (2004) the carbonation reaction is optimum when the RH in the pores of the matrix is close to 65% and decreases as the RH in the pores increases. The reaction is quasi-inhibited when the RH is below ca. 50%. K_2CO_3 appears to be a suitable salt to maintain an appropriate level of RH during the carbonation operation.

Owing to the cement's bleeding effect when water is present and which occurs in the early stages after casting, the porosity and pore size distribution is expected to vary between the top (trowelled) layer and deeper layers of the paste (Khatib, 2003). The trowelled face is located on the top of specimens and each face is identified as shown in Figure 23.

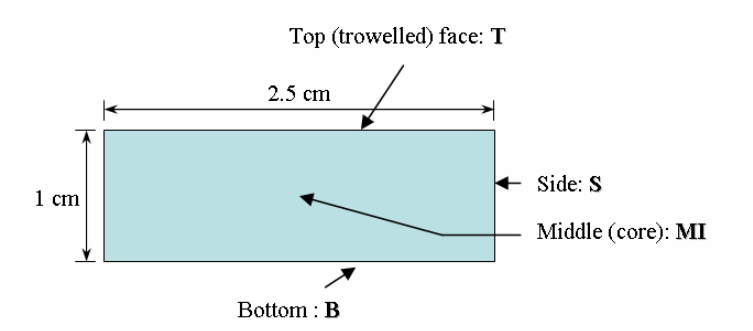

Figure 23: Identification of faces for carbonation operation (section through vertically cast cube)

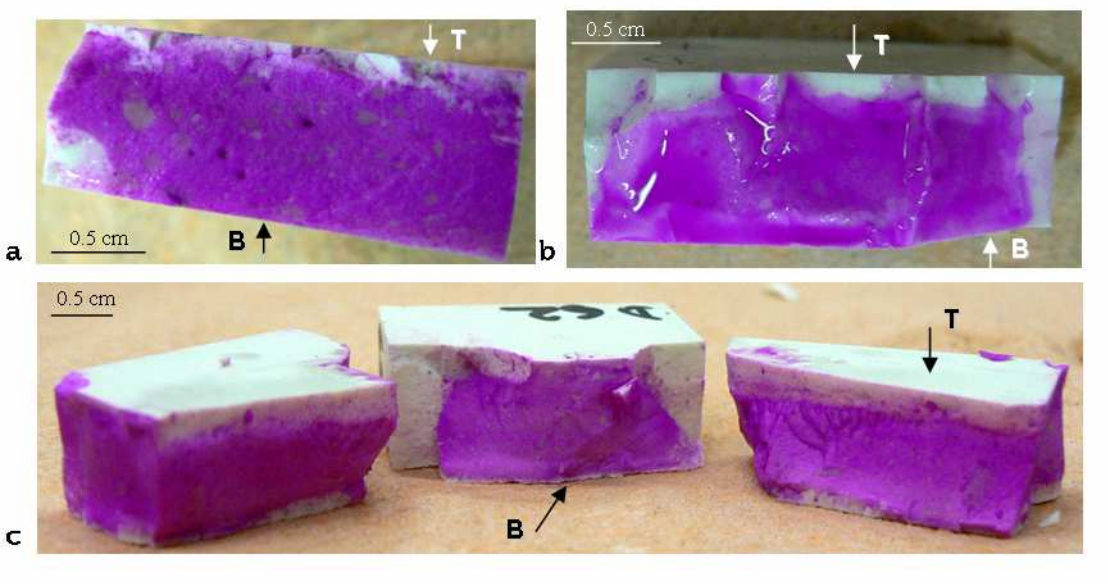

Figure 24: Carbonation depth for hydrated cement pastes after 48h of accelerated carbonation – Example of: (a) non pre-dried specimen, (b) and (c) pre-dried specimen

Figure 6 shows that the pre-dried specimens (Figure 24 b, and c) are more carbonated than those without pre-treatment (Figure 24 a). These observations are in accord with those previously reported. The formation of calcium carbonate requires that carbon dioxide diffuses from the atmosphere into the pores of material. This gas needs liquid water to form carbonic acid. However, the carbonation will be largely ruled out if the pore system is completely filled with water, which will hinder or block the diffusion of carbon dioxide in its gaseous phase. Thus, the situation where pores are only partly filled with water makes possible both diffusion of carbon dioxide in the gaseous phase and formation of carbonic acid (Rougeau, 1997; Johannesson et al., 2001; Gervais et al., 2004; Thiery, 2007).

The same carbonation profile (Figure 24 b) is observed for all pre-dried specimens whatsoever its location inside the chamber: both the top faces and sides are carbonated on about 1.5-2 mm whereas the bottom is almost non carbonated. The top surface (trowelled) of a cement paste possesses more numerous pores with often larger volume than the bottom face. The pore volume near the top surface can be twice as large as that for the bottom face (Khatib et al., 2003), which facilitates CO_2 penetration. In the following experiment the carbonated specimens used are pre-dried.

The results of carbonation influence on the matrix microstructure are presented and discussed in section 3.

2.2. Leaching operation

Leaching occurs in which species such as calcium exit dissolve in the pore solution, This phenomenon leads to an increase of the matrix pore volume (Watanabe et al., 2006). The leaching operation is performed on carbonated specimens. Leachate pH and surface pH of the matrix as a function of time are shown in Figure 25. Relating to the leachate pH curve, note that pH increases rapidly from about 5.5 to 9.2 in the first hours, reaches a maximum at 9.6 after 3 days, and then decreases slowly to about 8.5 after 28 days. On the contrary, the surface pH of the matrix decreases rapidly from ~10.6 to 9.3 during the first 3 days, and then decreases slowly and seems to reach a plateau around 8.8.

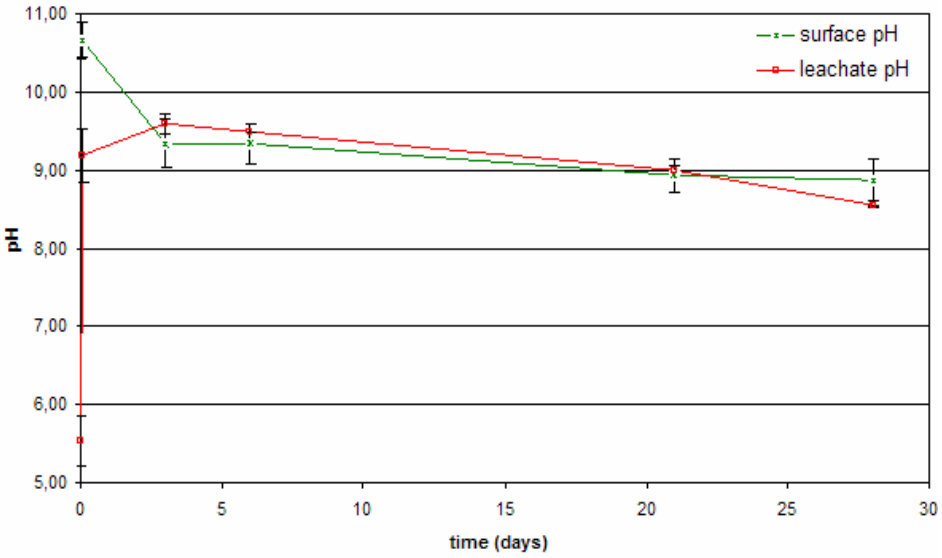

Figure 25: Evolution of pH in function of the leaching period (average of duplicates) - green curve: surface pH of the matrix, red curve: leachate pH

Prior to the leaching operation, specimens were carbonated for only 48h, and portlandite and ettringite remained present near the matrix surface (Figure 27). When specimens are submerged in water, soluble alkaline compounds, such as portlandite and ettringite, are rapidly dissolved. This results in the release of hydroxide ions and thereby increasing leachate pH and decreasing the surface pH of the matrix. In addition, portlandite dissolution involves the release of calcium (Ca) in leachate. The calcium concentration measured in leachate oscillates between 3.9 and 6.3 mg/L ($-4.4 < \log(Ca) < -4.2$). Calcium carbonate is much less soluble than portlandite (Figure 26), so once all portlandite is dissolved, local quasi-stationary state between the matrix pore solution and leachate progressively takes place. This is

consistent with the slow decrease in pH, calcium carbonate solubility and carbonate equilibria (Figure 26, calculations relating the considered system are detailed in annexe).

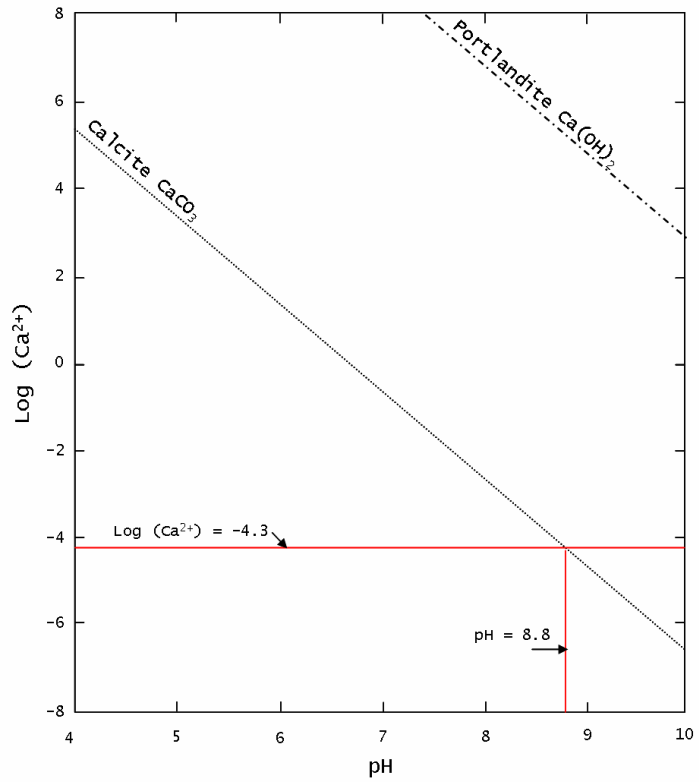

Figure 26: Soluble Calcium derived from calcite and portlandite for $CaCO_3$-$C0_2$-H_2O system – calcium carbonate in water with a fixed partial pressure of carbon dioxide (Bureau and Zasoski, 2002)

According to the curves of the Figure 26, pH should certainly decrease even more with time. Our objective is to accelerate the weathering of the matrix in order to decrease the surface pH. Hence, we have to find a compromise between the experimental time and pH obtained, that's why we decided to stop the experiment at 28 days corresponding to a surface pH about 8.8. The influence of leaching on the matrix microstructure is discussed in the next section.

3. Influence of accelerated weathering on the matrix microstructure

3.1. X-ray diffraction analysis

Figure 27 shows the XRD analysis performed on non weathered and weathered specimens. Additional peaks are noticed on the diffractogram of the carbonated specimen compared to non weathered one. They are attributed to the formation of calcium carbonate polymorphs – aragonite and vaterite – as a result of accelerated carbonation.

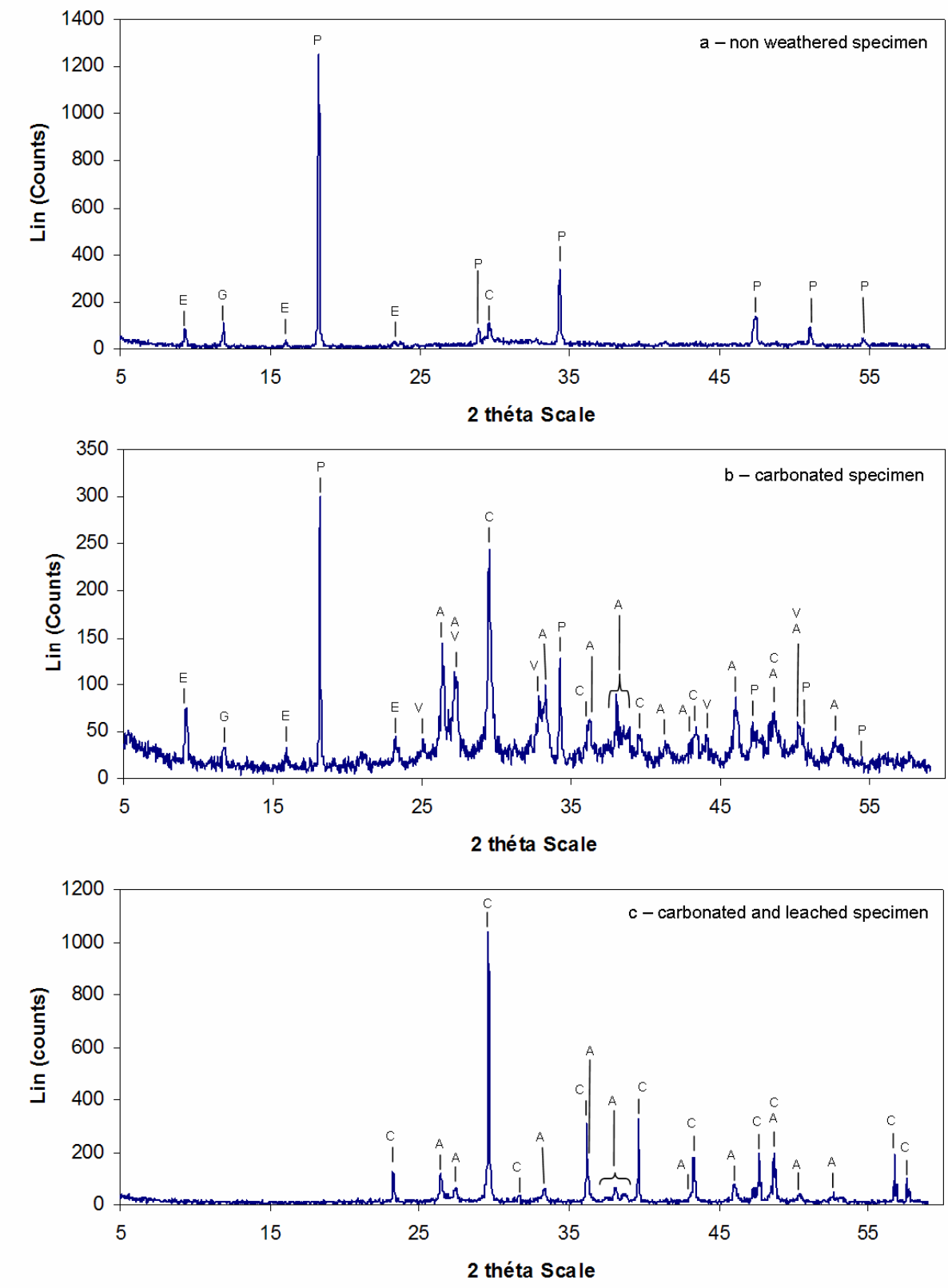

Figure 27: X-ray diffractogram of specimen before (a) and after (b), (c) accelerated weathering of the matrix – E=ettringite, G=gypsum, P=portlandite, C=calcite, A=aragonite, V=vaterite

The decrease in relative intensity of portlandite peaks is due to the dissolution of portlandite to form calcium carbonate. The diffractogram of the carbonated and leached specimen exhibits only calcite and aragonite peaks. The disappearance of portlandite and ettringite is a consequence of their dissolution as a result of leaching. Vaterite is the less stable calcium carbonate polymorph, and it is easily transformed into other forms.

3.2. Fourier Transformed Infrared analysis

The major bands identified for the non weathered specimen are: the OH band at 3636 cm^{-1} from portlandite, the carbonates bands at 1414, 875, and 710 cm^{-1} from calcite, and the silicate band at 959 cm^{-1} from C-S-H. The spectral data changes upon weathering and analyses of these changes can provide valuable information about the reactions involved. The FT-IR data for band assignments are presented in Table 3. Details of FT-IR spectra for the most characteristic bands are shown in Figure 28.

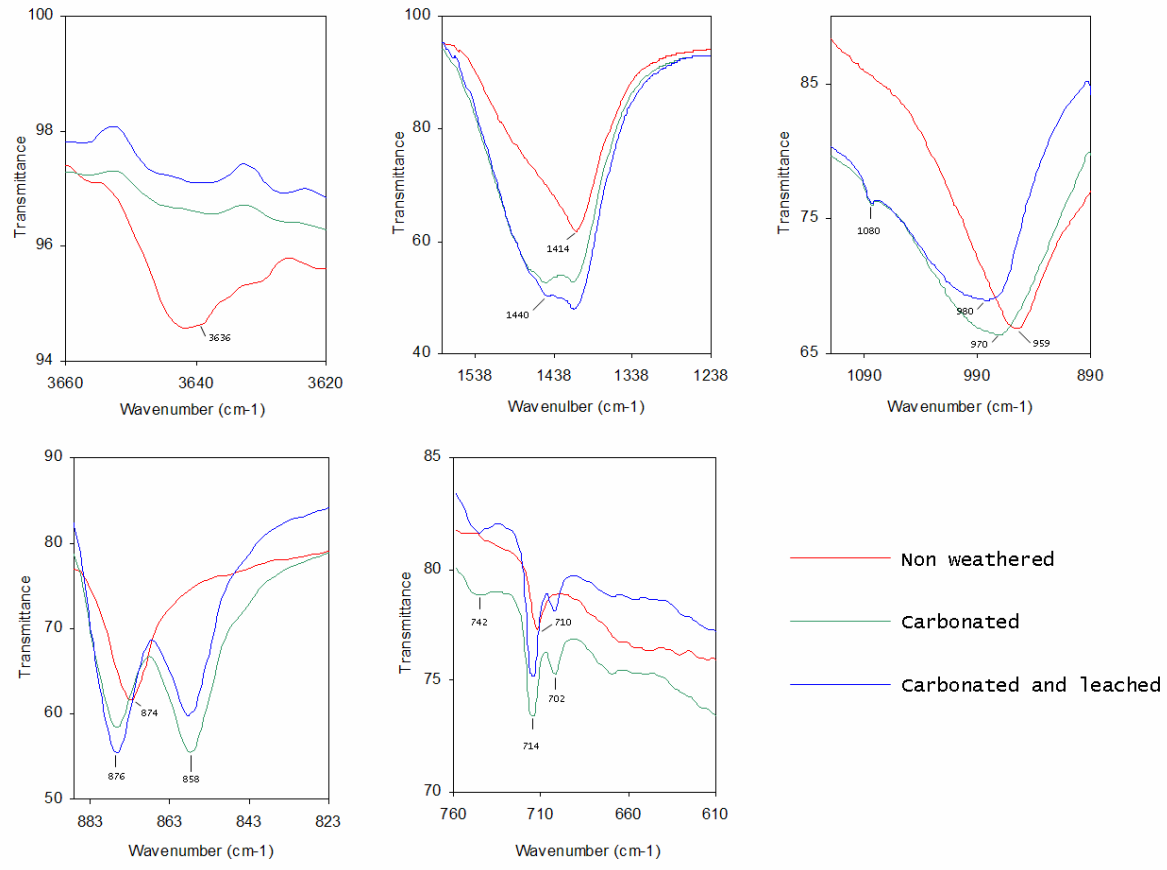

Figure 28: Details of FT-IR spectra (ATR) of the cementitious matrix before and after accelerated weathering

Table 3: FT-IR characterization of specimens before and after accelerated weathering

Band assignements	Calcium carbonate [a] $CaCO_3$ (cm^{-1})	Non weathered [b] specimen (cm^{-1})	Carbonated [c] specimen (cm^{-1})	Carbonated and [d] leached specimen (cm^{-1})
ν_3 SiO_4^{4-}	970 s, b	959 s	970 s	970 s
ν_2 SiO_4^{4-}	------	446 w	------	------
ν_3 SiO_4^{2-}	1100	1113 vw, sh	------	------
ν OH^-	3640 sr	3636 sh	------	------
ν_3 CO_3^{2-} calcite	1421 s, b	1414 s	1414 s	1414 s
ν_3 CO_3^{2-} aragonite	1400-1500 s, b		1414 - 1440 s, b	1414 - 1440 s, b
ν_1 CO_3^{2-} vaterite	1080 w	------		
ν_1 CO_3^{2-} aragonite	1083	------	1080 w, sh	1080 w, sh
ν_2 CO_3^{2-} calcite	874 m, sr	875 s, sr	876 s, sh	876 s, sh
ν_2 CO_3^{2-} vaterite	860 s, sr	------	?	?
	850 m, sr	------	?	?
ν_2 CO_3^{2-} aragonite	856 m	------	858 s, sh	858 s, sh
ν_4 CO_3^{2-} calcite	713 w	710 w	714 m	714 m
ν_4 CO_3^{2-} vaterite	740 w	------	742 w, sh	------
	710 m	------	?	?
ν_4 CO_3^{2-} aragonite	700	------	702 w	702 w

[a] References Simpson, 1997; Ghosh, 1998; Farcas and Touzé, 2001; Devarajan et al., 2007
[b] Present study - Non weathered specimen
[c] Present study - Carbonated specimen
[d] Present study - Carbonated and leached specimen
b: broad, s: strong, sh: shoulder, sr: sharp, m: medium, vw: very weak, w: weak
ν_1 = symmetric stretching
ν_2 = symmetric bending
ν_3 = asymmetric stretching
ν_4 = asymmetric bending
? = certainly covered by another band

The OH band at 3636 cm^{-1} from portlandite disappears with carbonation. However, XRD analyses show the presence of portlandite on carbonated specimen, but in small amounts. The majority of portlandite is mainly transformed during carbonation operation, and totally during leaching. The small amounts present on the carbonated specimen are probably non detectable with FT-IR.

The FT-IR spectra of weathered specimens (carbonated and leached or carbonated only) show a strong broad band at 1414-1440 cm^{-1}, which is broader than the calcite band, characteristic of aragonite. According to the intensity it can be assumed that the aragonite overlays the calcite band. New bands appear at 1080, 858, 702 cm^{-1} and are assigned to aragonite formed as a result of accelerated carbonation. The band at 742 cm^{-1} belonging to vaterite, appears only in the carbonated specimen. Other characteristic bands at 860, 850, and 710 cm^{-1} may be overlaid by calcite bands. As aforementioned, vaterite is a less stable polymorph of calcium carbonate and thereby transforms into more stable forms calcite and aragonite with leaching operation. The Si-O stretching (ν_3) band now appears at approximately 970 and 980 cm^{-1} for

the carbonated and carbonated then leached specimens respectively, while the same band in the non weathered specimen appears at 959 cm^{-1}. Hence, this shifting to higher frequency is caused by the polymerization of the orthosilicate units (SiO_4^{4-}) during weathering process. The magnitude of this shift is indicative of the degree of polymerization (Mollah et al., 1995).

3.3. Mercury Intrusion Porosity and helium pycnometry

The measured porosities vary from approximately 21% for the non weathered specimen to 17% for the carbonated one (Table 4). The leaching of hydrated cement pastes leads traditionally to an increase of the porosity. In our case, it doesn't. The leaching takes place after the carbonation, and a slight decrease of porosity is even noted.

The decrease in total porosity results in an increase of skeletal density. Well-defined threshold diameters are evident from 2 µm for the non weathered specimen to 500 and 400 nm for the carbonated and the carbonated then leached specimens respectively. Increased weathering time results in lower total porosity and smaller values for threshold diameter (Figure 29). The threshold diameter is a characteristic property of the pore structure and therefore varies with the microstructure of the material (Arandigoyen, 2006). A lower threshold value is indicative of a finer pore size distribution (Khatib, 2003). The lower threshold observed for the weathered specimens is a consequence of the disappearance of large pores around 1µm.

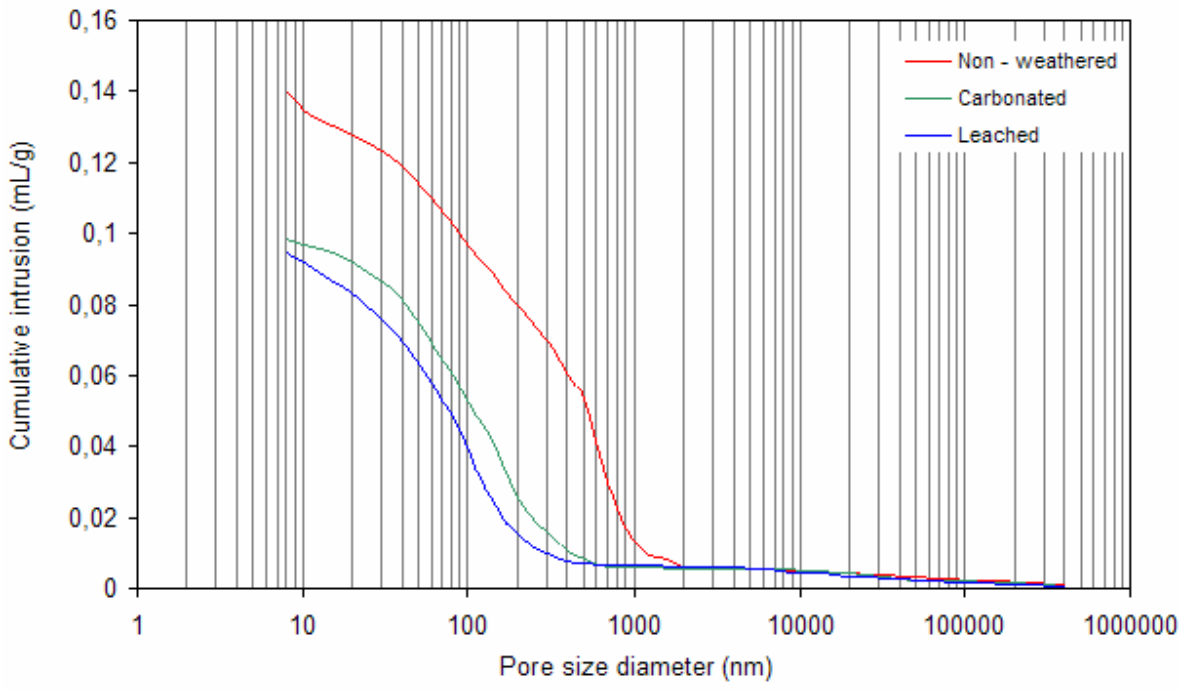

Figure 29: Change over time for the pore size distribution with accelerated weathering

Table 4: Characterization of the matrix microstructure

Specimen	Threshold diameter (nm)	Porosity (%)	Skeletal density (g/cm^{-3})
Non weathered	2000	21.6	2.1968
Carbonated	500	17.2	2.3352
Carbonated and leached	400	16.8	2.5383

The overall shape of the carbonated and leached or carbonated only curves is similar for weathered specimens, but differs from those of non weathered specimens. Beyond the threshold of the curve for the non weathered specimen (i.e. from approximately 2000 nm to 500 nm) there is a more profound decrease in the slope than for weathered specimens curve. But after a pore diameter of approximately 500 nm the slope increases again. This change in shape of the pore size distribution is a consequence of the increase in the proportion of smaller pores (Figure 29).

3.4. Direct observations

Figure 30 shows direct observations of specimens at different stages of accelerated weathering. The appearance of cracks on the surface specimen is observed after carbonation. This cracking is considerably augmented by leaching. Moreover, precipitate formation was noted inside the cracks, which according to XRD and FT-IR analysis should be $CaCO_3$.

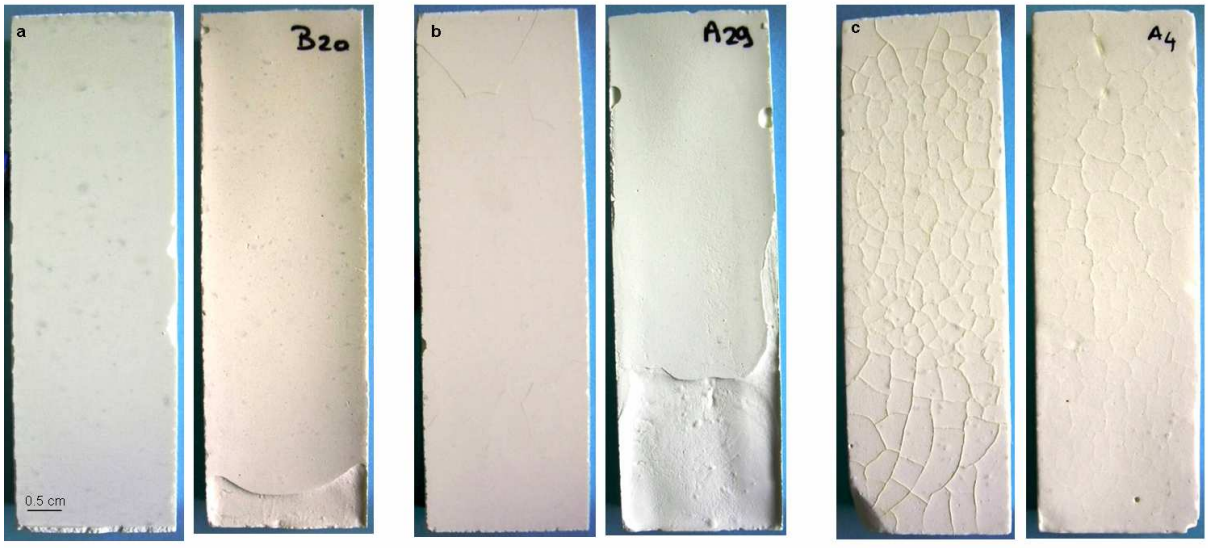

Figure 30: Direct observations of specimen before and after accelerated weathering – (a) non weathered specimen, (b) carbonated specimen, (c) carbonated then leached specimen

These observations point out the significant alterations of the specimen surface after the accelerated weathering.

3.5. Scanning Electron Microscope (SEM) observations

Figure 31 shows surface fractures. Platy crystals and fine needles are the distinguishing characteristic shapes of portlandite and ettringite respectively (Diamond, 1976; Pratt, 1986). A thin layer covers progressively the specimen surface as accelerated weathering progresses. This is consistent with the weathering performed: carbonation results in a decrease in the amount of portlandite and the leaching gives rise to the dissolution of portlandite and ettringite. A net decrease in porosity is also observed: pores are progressively filled by $CaCO_3$ precipitation and become smaller and smaller as the matrix is weathered.

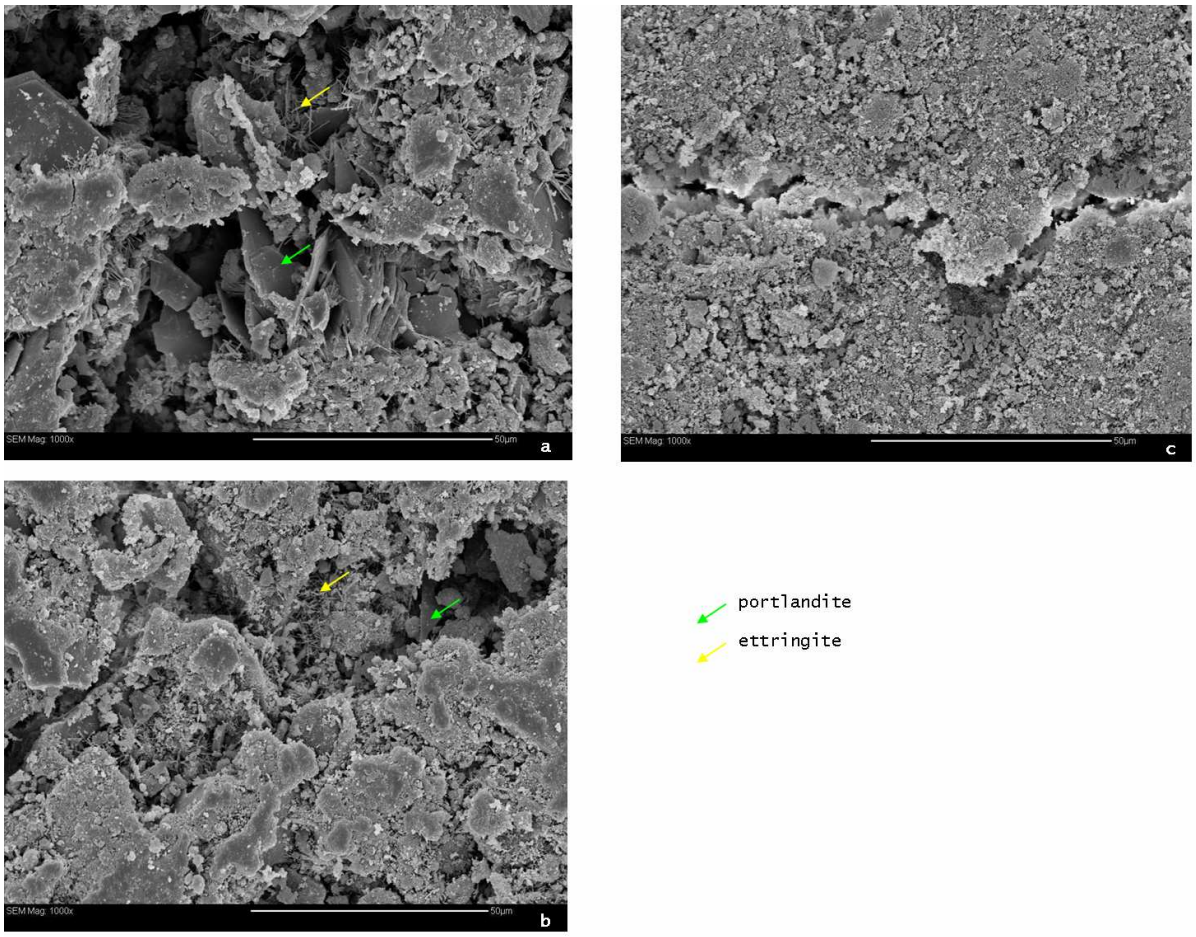

Figure 31: SEM images of fracture surfaces – (a) non weathered specimen, (b) carbonated specimen, (c) carbonated then leached specimen

Now, if one examines the following images of thin sections, microstructure alteration is not observed between non weathered and carbonated specimens (Figure 32 a and b, Figure 34 a and b). Contrarily, numerous cracks are observed for the carbonated and leached specimen (Figure 32 c). These cracks are distributed along the periphery (Figure 33). This phenomenon may be explained by one of two scenarios: (i) the cracks appear progressively during leaching operation, this could be confirmed by direct observation (Figure 30 c) or (ii) the matrix structure is weakened by the leaching operation, and thereby the cracks are due to the sample preparation. We also notice on the carbonated and leached sample the presence of a thin band which seems to be more porous than the rest of specimen (Figure 32 c, Figure 34). Its thickness is estimated to be 70 µm (Figure 34).

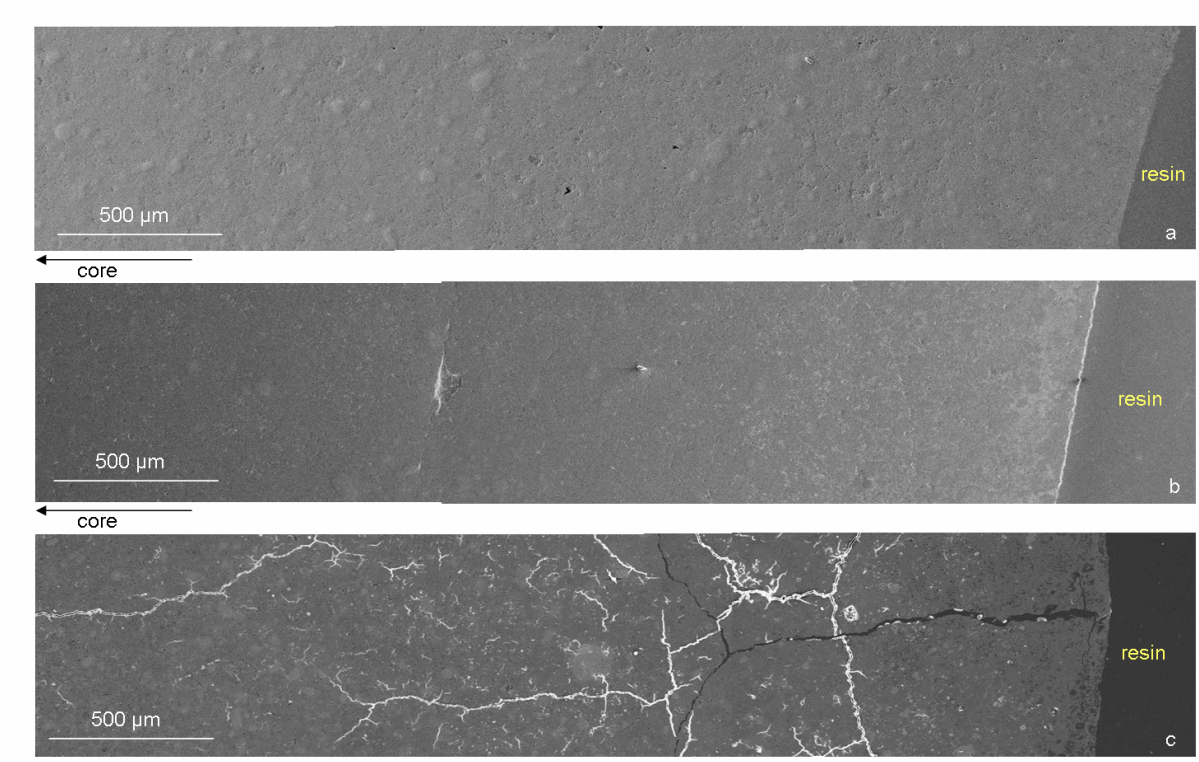

Figure 32: SEM images of thin sections – (a) non weathered specimen, (b) carbonated specimen, (c) carbonated and leached specimen

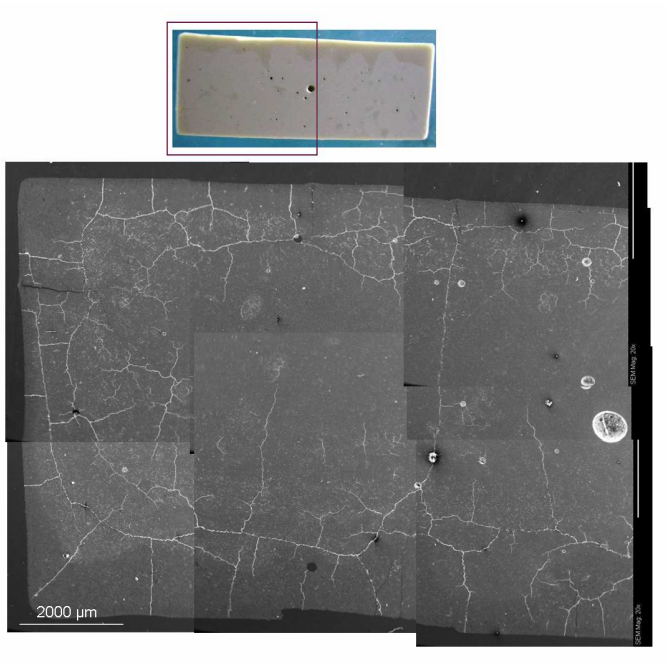

Figure 33: Global SEM images of thin sections of a carbonated and leached specimen

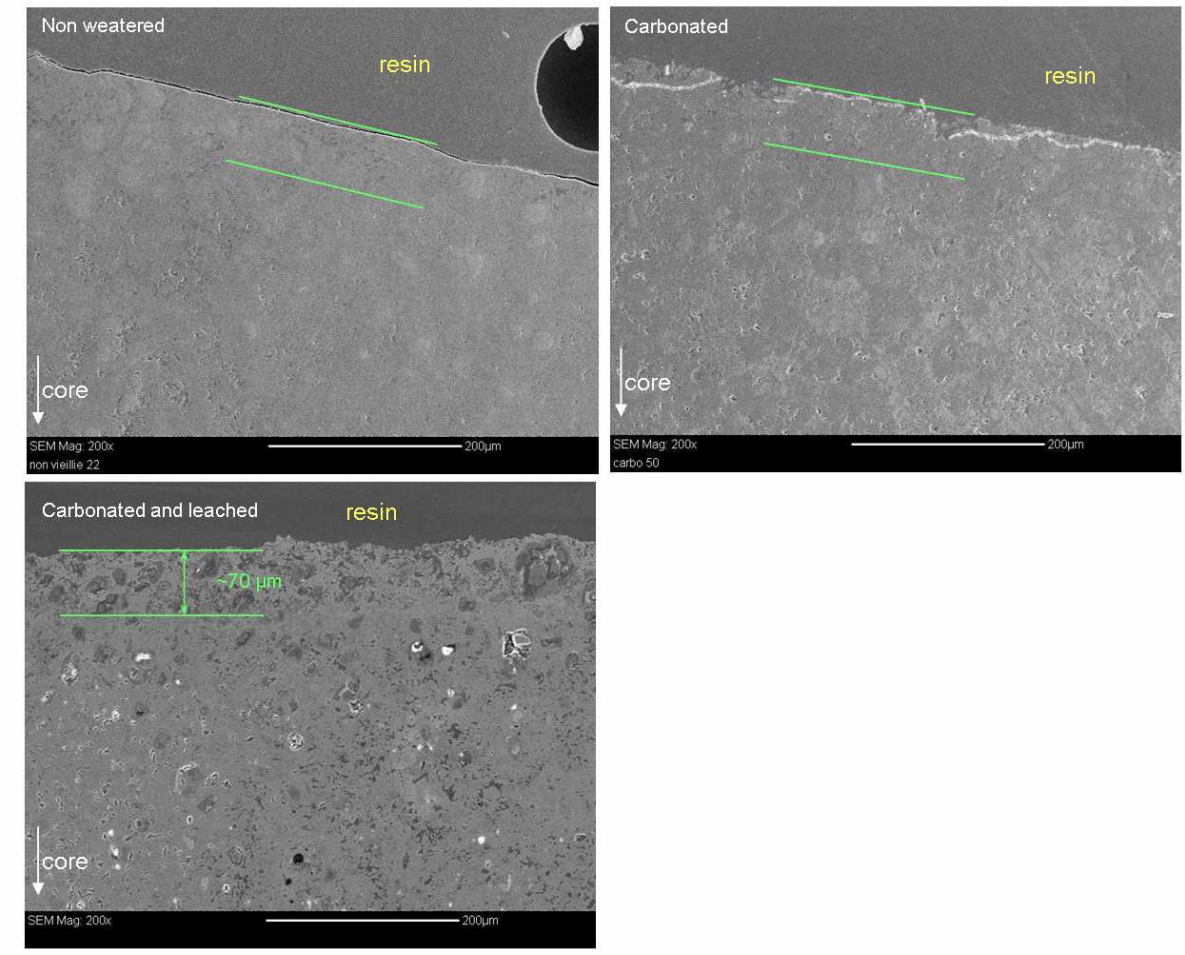

Figure 34: Measured thickness in close ups of earlier images

3.6. SEM/EDX analysis

Direct and microscopic observations point out surface alterations and changes in microstructure of carbonated and leached specimens. Hence, chemical change was expected from EDX analysis. Figure 36 presents EDX analysis performed on carbonated and leached specimens, and Figure 35 shows the different areas analysed. Twenty punctual analyses are performed for each area, mean values are plotted on graphs. Each analysis is performed on a surface about 20 x 200 µm.

We compare concentrations in calcium, silicon, aluminium between analyses performed on the side and in the core. We assume that accelerated weathering has a superficial impact, so the chemical composition in the core is representative of a non weathered matrix. This was confirmed with comparison with analyses performed on non weathered specimens.

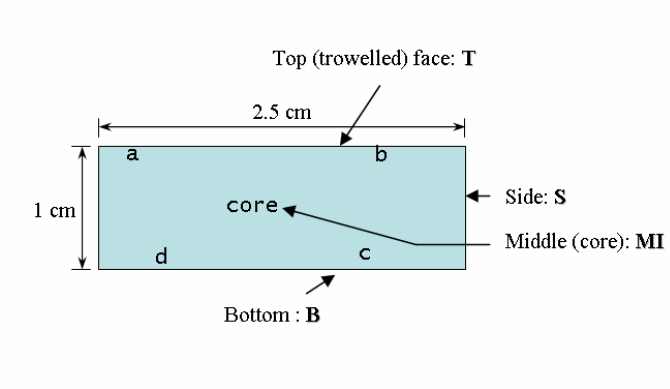

Figure 35: Localization of EDX analyzed areas

EDX data shows no change in chemical composition, there is just a tendency of Ca enrichment and thereby Si depletion on the sides of specimen

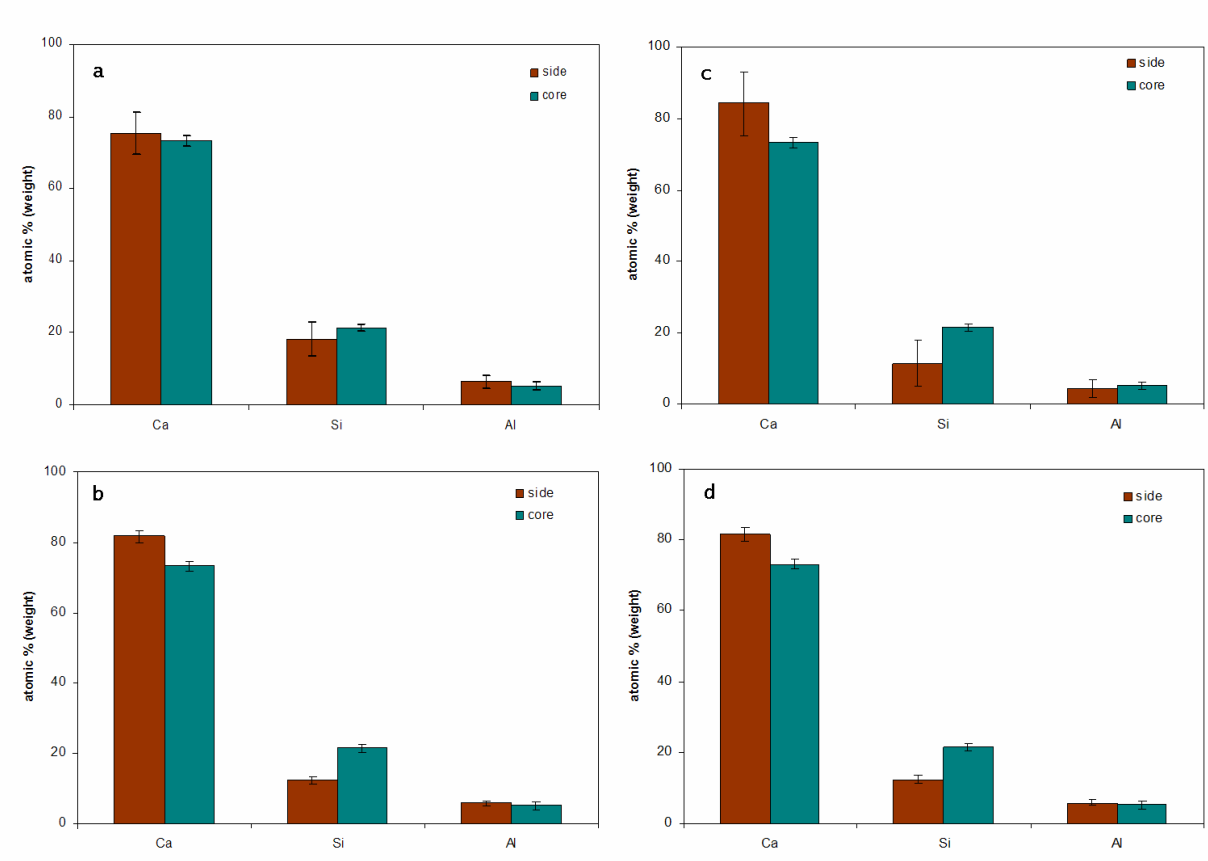

Figure 36: SEM / EDX analysis of thin sections for carbonated and leached specimen

3.7. Discussion

Our results show that accelerated carbonation results in calcite, vaterite and aragonite formation (Figure 27, Figure 28). This is consistent with literature. The presence of metastable forms (vaterite and aragonite) in the carbonated area seems to be a feature of accelerated carbonation tests (Thiery et al., 2007). According to Thiery (2005), the thermal stability of $CaCO_3$ produced is lower as the carbonation level increases. This author also showed that the thermodynamically metastable forms of $CaCO_3$ correspond to the carbonation of C-S-H. The shift of the $\nu_3SiO_4^{4-}$ from the FT-IR spectrum (Figure 28) to higher wave number units suggests also a polymerisation of C-S-H with the carbonation as well as with leaching operations (Mollah et al., 1995).

The carbonation reaction mainly has two effects on the cement matrix and its pore water solution (Van Gerven et al., 2004): lowering of the pH of the pore water, and decreasing of the matrix porosity. This is because of the formation of calcite, which is less dense than portlandite, thereby can clog pores more easily. A decrease of total porosity of about 20% is noticed with accelerated weathering (Table 4). The porosity decrease observed in literature

ranged from 10 to 19 % (Houst and Wittmann, 1994; Ngala and Page, 1997). Evolution of total porosity with carbonation is dependent of w/c ratio and cement type.

The presence of cracks for weathered specimen is not detected with MIP analyses. This can be explained by the sampling method used. Specimens are broken into small pieces. They break along cracks, so these fissures don't appear in the final sample.

Generally, the leaching of cement paste gives rise to matrix decalcification due to the dissolution of portlandite and C-S-H decalcification. Haga et al. (2005) concluded from their work that the major leached constituents of hardened ordinary Portland cement are portlandite and C-S-H gel, and the large pore size, associated with the leaching of portlandite, will significantly affect the diffusion of leached constituents. An increase in porosity was expected after the leaching of our carbonated specimen from the dissolution of portlandite and the transformation of vaterite into calcite (Thiery et al., 2007). However, results show a slight decrease in total porosity after leaching operation (Table 4). In the present study leaching occurs after carbonation. The porosity decrease diminishes the leaching of matrix constituents, while the decrease in pH increases leaching. The effect of porosity, however, exceeds that of pH, resulting in a net decrease of leaching due to carbonation (Van Gerven et al., 2007). It can be assumed that the dissolution of portlandite and decalcification of C-S-H result in $CaCO_3$ precipitation in the pore volume. Gervais (1999) found that carbonation prior to leaching operation results in a decrease of calcium release compared to the leaching of non carbonated specimens. The mobility of Ca^{2+} is reduced, and it may precipitate with CO_3^{2-} before, thus not reaching leachate. This could explain EDX analyses and lack of the matrix decalcification observed (Figure 36): most of the dissolved Ca^{2+} precipitates into $CaCO_3$ before, hence not exiting the matrix with the outcome: an enrichment in calcium near the specimen surface.

4. Conclusion

To conclude, the key points to remember are:

- Accelerated weathering of the matrix alters the general surface aspects of the specimens.
- Carbonation of specimen leads to a decrease of the surface pH and total porosity, as well as the formation of calcite, vaterite and aragonite as a result of the depletion of portlandite, and polymerization of C-S-H respectively.

- Carbonated and leached specimens are characterized by a lower surface pH and lesser porosity than carbonated only. They are mainly composed by calcite, aragonite and C-S-H gel.